

RESEARCH ARTICLE

A comprehensive assessment of physical image quality of five different scanners for head CT imaging as clinically used at a single hospital centre—A phantom study

Patrizio Barca^{1‡}, Fabio Paolicchi², Giacomo Aringhieri², Federica Palmas³, Daniela Marfisi¹, Maria Evelina Fantacci^{3,4}, Davide Caramella², Marco Giannelli^{1*}

1 Unit of Medical Physics, Pisa University Hospital “Azienda Ospedaliero-Universitaria Pisana”, Pisa, Italy, **2** Diagnostic and Interventional Radiology, University of Pisa, Pisa, Italy, **3** Department of Physics, University of Pisa, Pisa, Italy, **4** INFN, Pisa section, Pisa, Italy

‡ Current address: Department of Medical Physics, St. Orsola-Malpighi University Hospital, Bologna, Italy
* m.giannelli@ao-pisa.toscana.it



OPEN ACCESS

Citation: Barca P, Paolicchi F, Aringhieri G, Palmas F, Marfisi D, Fantacci ME, et al. (2021) A comprehensive assessment of physical image quality of five different scanners for head CT imaging as clinically used at a single hospital centre—A phantom study. *PLoS ONE* 16(1): e0245374. <https://doi.org/10.1371/journal.pone.0245374>

Editor: Guillem Pratz, Stanford University School of Medicine, UNITED STATES

Received: February 24, 2020

Accepted: December 28, 2020

Published: January 14, 2021

Copyright: © 2021 Barca et al. This is an open access article distributed under the terms of the [Creative Commons Attribution License](https://creativecommons.org/licenses/by/4.0/), which permits unrestricted use, distribution, and reproduction in any medium, provided the original author and source are credited.

Data Availability Statement: The CT data are held on a public repository (Harvard Dataverse) and are freely available at <https://doi.org/10.7910/DVN/TSSN77>.

Funding: The authors received no specific funding for this work.

Competing interests: The authors have declared that no competing interests exist.

Abstract

Nowadays, given the technological advance in CT imaging and increasing heterogeneity in characteristics of CT scanners, a number of CT scanners with different manufacturers/technologies are often installed in a hospital centre and used by various departments. In this phantom study, a comprehensive assessment of image quality of 5 scanners (from 3 manufacturers and with different models) for head CT imaging, as clinically used at a single hospital centre, was hence carried out. Helical and/or sequential acquisitions of the Catphan-504 phantom were performed, using the scanning protocols (CTDI_{vol} range: 54.7–57.5 mGy) employed by the staff of various Radiology/Neuroradiology departments of our institution for routine head examinations. CT image quality for each scanner/acquisition protocol was assessed through noise level, noise power spectrum (NPS), contrast-to-noise ratio (CNR), modulation transfer function (MTF), low contrast detectability (LCD) and non-uniformity index analyses. Noise values ranged from 3.5 HU to 5.7 HU across scanners/acquisition protocols. NPS curves differed in terms of peak position (range: 0.21–0.30 mm⁻¹). A substantial variation of CNR values with scanner/acquisition protocol was observed for different contrast inserts. The coefficient of variation (standard deviation divided by mean value) of CNR values across scanners/acquisition protocols was 18.3%, 31.4%, 34.2%, 30.4% and 30% for teflon, delrin, LDPE, polystyrene and acrylic insert, respectively. An appreciable difference in MTF curves across scanners/acquisition protocols was revealed, with a coefficient of variation of f_{50%}/f_{10%} of MTF curves across scanners/acquisition protocols of 10.1%/7.4%. A relevant difference in LCD performance of different scanners/acquisition protocols was found. The range of contrast threshold for a typical object size of 3 mm was 3.7–5.8 HU. Moreover, appreciable differences in terms of NUI values (range: 4.1%–8.3%) were found. The analysis of several quality indices showed a non-negligible variability in head CT imaging capabilities across different scanners/acquisition protocols. This highlights the

importance of a physical in-depth characterization of image quality for each CT scanner as clinically used, in order to optimize CT imaging procedures.

1. Introduction

In recent years, the extraordinary technical advances in x-ray computed tomography (CT) have largely increased its use in the clinical practice. Thus, CT has become a fundamental imaging tool in several body as well as head applications, providing useful information for diagnosis and patient care [1–3].

Given that CT imaging represents the largest source of population exposure to ionizing radiation in industrialized countries [4, 5] and increased radiation dose may increase the risk of cancer [6], it is important to minimize radiation dose (without compromising the diagnostic potential) through an optimization and standardization of acquisition protocols [7–9]. Accordingly, various technical approaches (e.g. tube current modulation, automatic exposure control, iterative reconstruction algorithms) to optimize CT acquisitions in various applications can be used [10–15]. Furthermore, some previous studies have described phantom-based methods to optimize acquisition protocol for specific CT imaging techniques and applications, exploiting various physical image quality indices [9, 16–21]. For instance, Zhang et al [9] have developed a CT protocol optimization platform by combining task-based detectability calculations with a graphical user interface that demonstrates the trade-off between dose and image quality. Their platform can be used to improve individual dose efficiency and acquisition protocol consistency across various patient sizes and CT scanners. Berta et al [19] have described a method to objectively evaluate image quality when new clinical protocol performances must be compared with a standard reference. This quantitative approach has been applied to the images of a typical routine abdominal protocol, which were reconstructed with the standard filtered back projection (FBP) and the Iterative Reconstruction in Image Space (IRIS) algorithm. An adaptable and global approach for optimizing CT protocols, by evaluating the influence of acquisition parameters and iterative reconstruction algorithms, has been proposed and implemented in a software program by Greffier et al [20]. Moreover, Noferini et al [21] have proposed and validated a method that employs a Channelling Hotelling model Observer in a CT protocol optimization program, with the aim at assuring that scanners are working at their own best with regard to image quality and patient exposure.

Nonetheless, an objective and in-depth physical characterization of performance of CT scanners [22–29], acquisition methods [30–35] and image reconstruction algorithms [36–41], in terms of specific quantitative image quality indices, remains an essential step. Indeed, these indices have the potential to serve as a basis for guiding and optimizing clinical protocols [42–44]. In this regard, previous phantom studies have shown that CT image quality can vary substantially when acquisitions are performed on different scanners [45–48], even using similar acquisition protocols [49–52]. Therefore, a careful assessment of image quality for each specific CT imaging technique and application is recommended.

Given also time efficiency and cost considerations, head CT is a first line imaging examination for assessing neurological disorders [53–55]. In particular, head CT imaging is highly sensitive to bleeding, and is an essential diagnostic modality to investigate osseous structures as well as to detect calcifications. Moreover, it is usually preferred to magnetic resonance imaging for its wide availability, rapid acquisition and high spatial resolution [56, 57]. In this regard, 5 CT scanners, with different technical characteristics, are currently installed at our hospital

centre. It should be noted that radiologists and neuroradiologists by various departments of our institution execute head CT examinations on these scanners by using different acquisition protocols, with similar radiation dose values. Therefore, toward an optimization of CT imaging procedures at our hospital centre, the aim of this phantom study was to comprehensively assess whether and how head CT physical image quality varies with different scanners as clinically used for routine examinations.

2. Materials and methods

2.1. Scanners and phantom acquisitions

Images of the Catphan-504 phantom (The Phantom Laboratory, NY, USA) were acquired on 5 CT scanners (one 128-slice, two 64-slice and two 16-slice CT scanners) from different manufacturers (Table 1). The phantom has a cylindrical shape with a diameter of 20 cm and it is composed of four modules. In particular, the CTP486 and CTP404 modules of the phantom were employed for CT acquisitions. The CTP486 module is a homogeneous water-equivalent module, while the CTP404 module includes multiple inserts of different materials in a water-equivalent background (Fig 1). Nominal CT Hounsfield units (HU) values of the inserts are reported in Table 2.

Sequential and/or helical clinical CT head protocols, with different acquisition parameters but similar radiation doses in terms of $CTDI_{vol}$, were employed for acquisitions on CT scanners as indicated in Table 3. CT images were reconstructed by using the conventional filtered back-projection algorithm.

2.2. Physical image quality assessment

For each CT scanner/acquisition protocol, physical image quality was assessed through a number of indices which are strictly related to the main characteristics of images in terms of noise, spatial resolution and contrast properties [59–64]. In particular, quantitative metrics of noise level, noise power spectrum (NPS), contrast-to-noise ratio (CNR), modulation transfer function (MTF), low contrast detectability (LCD) and non-uniformity index (NUI) were estimated.

For each image quality index and CT scanner/acquisition protocol, 5 repeated acquisitions were performed. The estimated value and uncertainty of a quality index were obtained as the mean value and standard deviation (SD) across repeated measurements, respectively.

Image analysis was performed by using ImageJ (Wayne Rasband, National Institute of Health, USA), Origin (OriginLab Corporation, MA, USA) and Matlab (The MathWorks, Inc., MA, USA) software packages.

2.2.1. Noise level

Noise level was evaluated by computing the SD of HU values within a 4.5 cm diameter circular region of interest (ROI), placed at the centre of the acquisition slab central image of the uniform CTP486 module.

Table 1. CT scanners enrolled in the study.

Scanner ID	Manufacturer	Model	Number of slices
Toshiba-16	Toshiba Medical Systems, Japan	Aquilion 16	16
GE-16RT	GE Healthcare, USA	LightSpeed RT16	16
GE-64VCT	GE Healthcare, USA	LightSpeed VCT	64
Siemens-64	Siemens Healthineers, Germany	Sensation 64	64
GE-128	GE Healthcare, USA	Discovery 750 HD	128

<https://doi.org/10.1371/journal.pone.0245374.t001>

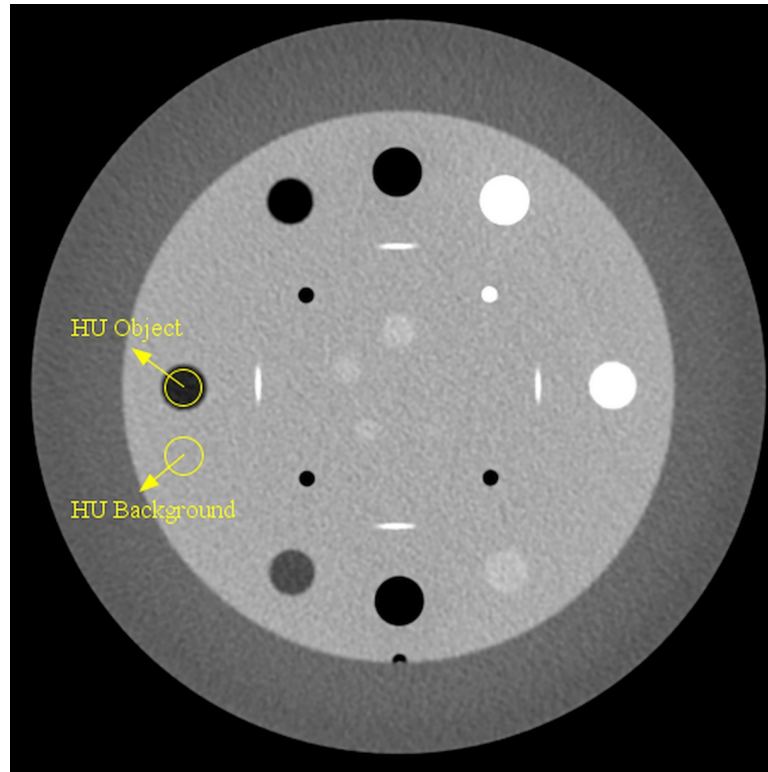


Fig 1. ROIs position for CNR evaluation in the CTP404 module of the Catphan-504 phantom. The depicted ROIs refer to the LDPE contrast insert.

<https://doi.org/10.1371/journal.pone.0245374.g001>

2.2.2. Noise power spectrum (NPS)

Texture properties of CT image noise were assessed by computing the NPS (i.e. the spatial frequency distribution of noise) [65, 66]:

$$NPS(f_x, f_y) = \frac{\Delta x \cdot \Delta y}{N_x \cdot N_y} \cdot \langle |FFT(ROI_{noise})|^2 \rangle \quad (1)$$

where f_x/f_y are the spatial frequencies along the main orthogonal directions, $\Delta x/\Delta y$ are the voxel sizes, N_x/N_y are the number of voxels for each direction, FFT is the two-dimensional (2D) fast Fourier transform, $ROI_{noise}(x,y)$ is the local value of an "only-noise" ROI and $\langle \rangle$ indicates the ensemble average (i.e. the average across measurements performed on a number of ROIs). In particular, for each acquisition, an ensemble of 5 ROIs (64 pixels \times 64 pixels) was selected from the acquisition slab central image of the uniform CTP486 phantom module. Given the radial symmetry of the 2D NPS, radial profiles along many directions were averaged

Table 2. Nominal HU values of the Catphan-CTP404 module inserts [58].

Material	HU range (reference values)
LDPE	-121: -87
Polystyrene	-65: -29
Acrylic	92: 137
Delrin	344: 387
Teflon	941: 1060

<https://doi.org/10.1371/journal.pone.0245374.t002>

Table 3. Clinical head CT imaging protocols used for each scanner by the staff of various Radiology/Neuroradiology departments at the Pisa university hospital.

Scanner ID	Scan mode	Tube load (mAs)	Tube voltage (kVp)	Pitch factor	Slice thickness (mm)	S-FOV	Collimation (mm)	CTDI _{vol} (mGy)	Reconstruction kernel
Toshiba-16	h	165	120	0.688	4	M	16	56.6	FC64
	s	220	120	-	4	M	8	54.7	FC64
GE-16RT	s	330	120	-	2.5	head	10	57	Standard
GE-64VCT	s	320	120	-	5	head	20	57.5	Standard
Siemens-64	s	380	120	-	6	head	18	55.7	H31S
GE-128	h	280	120	0.969	5	head	20	56.1	Standard
	s	280	120	-	5	head	20	55.9	Standard

h = helical, s = sequential.

<https://doi.org/10.1371/journal.pone.0245374.t003>

in order to obtain the one dimensional NPS curve. In particular, the selection of radial profiles was carried out every 10° over 360°, obtaining a total of 36 radial profiles.

In order to estimate peak position, NPS curves were fitted by using a specific peak function (namely "InvsPoly") implemented in Origin:

$$f(x) = y_0 + \frac{A}{1 + A_1 \left(2 \frac{x-x_c}{w}\right)^2 + A_2 \left(2 \frac{x-x_c}{w}\right)^4 + A_3 \left(2 \frac{x-x_c}{w}\right)^6} \quad (2)$$

where x_c is the peak position, $A/A_1/A_2/A_3$ are coefficients related to the amplitude of the peak, w is a parameter related to the width of the curve and y_0 is an offset.

2.2.3. Contrast-to-noise ratio (CNR)

Images of different inserts (i.e. teflon, delrin, LDPE, polystyrene, acrylic) of the CTP404 phantom module, whose nominal HU values are reported in Table 2 [60], were used to estimate CNR. In particular, CNR was estimated as follows [67, 68]:

$$CNR = \frac{|HU_{obj} - HU_{bkg}|}{\sigma_{bkg}} \quad (3)$$

where HU_{obj} and HU_{bkg} are the mean of HU values in a circular ROI (diameter 9 mm) in the considered insert and background region, respectively, while σ_{bkg} is the SD of CT numbers in a background region close to the considered insert (Fig 1).

2.2.4. Modulation transfer function (MTF)

Spatial resolution was evaluated in the spatial frequency domain. The modulation transfer function (MTF) was computed through the circular edge method (i.e. starting from edge spread function measurements) as follows [65, 69]:

$$MTF(f) = \frac{\left| \int \frac{d}{dx} ESF(x) \cdot e^{-i2\pi fx} dx \right|}{\int \frac{d}{dx} ESF(x) dx} \quad (4)$$

where f and ESF represent the spatial frequency and edge spread function, respectively. In particular, ESF was referred to the teflon insert of the CTP404 phantom module [58]. The spatial frequencies corresponding to 50% ($f_{50\%}$) and 10% ($f_{10\%}$) of each MTF curve were estimated.

2.2.5. Low contrast detectability (LCD)

A low-contrast detectability (LCD) analysis was performed on the homogeneous module of the phantom (CTP486), using a statistical method [64, 70, 71] based on the Rose model of threshold signal detectability [72–75]. Specifically, squared ROIs ranging from 2×2 pixels to 11×11 pixels (i.e. object sizes approximately ranging from 0.85 mm to 4.75 mm) were employed in this analysis. A set of 900 ROIs (placed randomly and covering all phantom image) were analysed for each ROI size and the contrast threshold (C_t) was evaluated, by assuming a Gaussian distribution of the average of HU values within each ROI [64, 70, 71], as follows:

$$C_t(HU) = 3.29 \cdot \Delta \quad (5)$$

where Δ is the standard deviation of the Gaussian distribution, with mean value μ . Accordingly, a low contrast object of the same size as the ROIs can be revealed at a confidence level of 95% if its mean HU value differs more than 3.29Δ from μ [76].

2.2.6. Non-uniformity index (NUI)

Variation of CT numbers within acquisition slab central image of the uniform CTP486 module was assessed through the non-uniformity index (NUI). In particular, NUI was estimated by adapting the method proposed by Li et al and suggested by the AAPM TG233 report for assessing spatial non-uniformity of noise maps [38, 77]. Images of the entire phantom were divided into $M = 249$ small ROIs of $7 \text{ mm} \times 7 \text{ mm}$ size. Then, NUI index was calculated as:

$$NUI(\%) = \frac{100}{I} \sqrt{\frac{1}{M-1} \sum_{j=1}^M (I_j - I)^2} \quad (6)$$

where I_j and $\langle I \rangle$ are the average of CT numbers within the j -th ROI and average of all I_j values, respectively.

3. Results

Noise results are reported in Table 4. An appreciable difference in noise values across different scanners/acquisition protocols was found. Noise values ranged from 3.5 ± 0.1 HU (Siemens-64 scanner) to 5.7 ± 0.1 HU (GE-16RT scanner).

Fig 2 shows NPS curves for each scanner/acquisition protocol. NPS curves differed in terms of peak position (Table 5), with Toshiba-16 (both axial and helical scan mode) ($\sim 0.22 \text{ mm}^{-1}$)

Table 4. Noise (σ) values (mean \pm standard deviation across five repeated measurements), for each CT scanner/acquisition protocol.

Scanner ID	Scan mode	σ (HU)
Toshiba-16	h	4.2 ± 0.1
	s	4.6 ± 0.2
GE-16RT	s	5.7 ± 0.1
GE-64VCT	s	3.9 ± 0.1
Siemens-64	s	3.5 ± 0.1
GE-128	h	4.6 ± 0.1
	s	4.3 ± 0.1

h = helical, s = sequential.

<https://doi.org/10.1371/journal.pone.0245374.t004>

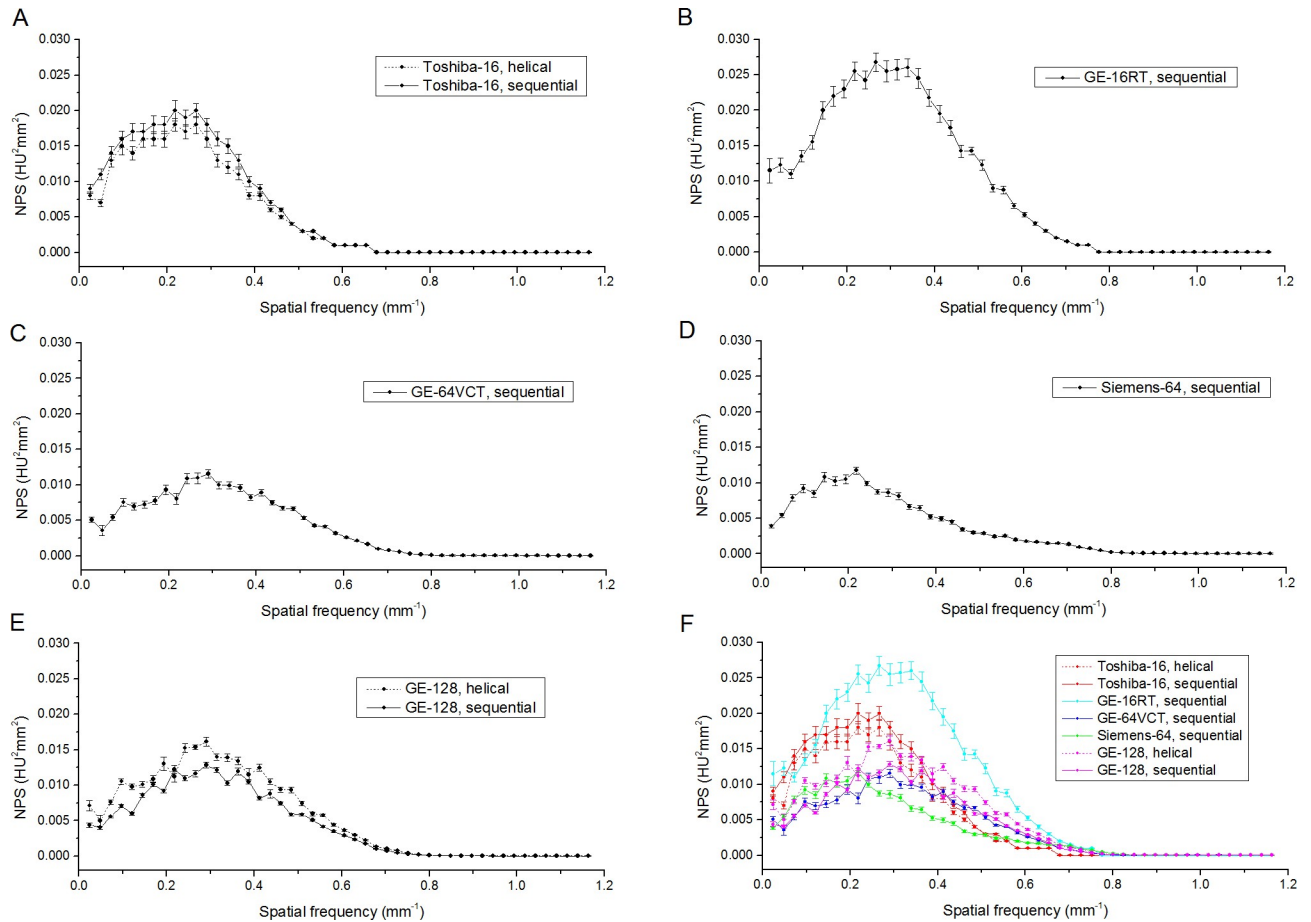


Fig 2. Noise power spectrum (NPS) of images acquired using different CT scanners/acquisitions protocols. Panels A, B, C, D and E show the NPS curves (mean ± standard deviation across five repeated measurements) for Toshiba-16, GE-16RT, GE-64VCT, Siemens-64 and GE-128 scanners, respectively. In order to better compare the different NPS curves, panel F shows on the same graphic the NPS curves for all scanners/acquisition protocols.

<https://doi.org/10.1371/journal.pone.0245374.g002>

and Siemens-64 (~ 0.21 mm⁻¹) scanners showing lower peak position with respect to the other scanners (> 0.29 mm⁻¹).

CNR results are reported in detail in Table 6. A substantial variation of CNR values with scanner/acquisition protocol was observed for all inserts (teflon, delrin, LDPE, polystyrene, acrylic). The coefficient of variation (standard deviation divided by mean value) of CNR values

Table 5. Peak position of NPS curves for each CT scanner/acquisition protocol.

Scanner ID	Scan mode	Peak position (mm ⁻¹)
Toshiba-16	h	0.22 ± 0.01
	s	0.22 ± 0.01
GE-16RT	s	0.29 ± 0.01
GE-64VCT	s	0.29 ± 0.01
Siemens-64	s	0.21 ± 0.01
GE-128	h	0.30 ± 0.01
	s	0.30 ± 0.01

h = helical, s = sequential.

<https://doi.org/10.1371/journal.pone.0245374.t005>

Table 6. CNR values (mean ± standard deviation across five repeated measurements) of different inserts from the CTP404 phantom, for each CT scanner/acquisition protocol.

Scanner ID	Scan mode	Teflon	Delrin	LDPE	Polystyrene	Acrylic
Toshiba-16	h	167 ± 6	44 ± 3	43 ± 3	31 ± 1	5.5 ± 0.6
	s	150 ± 20	38 ± 2	42 ± 4	28 ± 2	5.3 ± 0.5
GE-16RT	s	140 ± 11	41 ± 2	35 ± 2	23 ± 2	4.7 ± 0.5
GE-64VCT	s	209 ± 20	65 ± 8	54 ± 4	38 ± 4	7.4 ± 0.4
Siemens-64	s	233 ± 22	89 ± 6	73 ± 5	55 ± 2	10.6 ± 0.8
GE-128	h	200 ± 10	59 ± 3	31 ± 2	33 ± 1	6.2 ± 0.4
	s	177 ± 12	64 ± 5	31 ± 3	30 ± 3	6.4 ± 0.5

h = helical, s = sequential.

<https://doi.org/10.1371/journal.pone.0245374.t006>

across different scanners/acquisition protocols was 18.3%, 31.4%, 34.2%, 30.4% and 30% for teflon, delrin, LDPE, polystyrene and acrylic insert, respectively.

MTF results are shown in Fig 3 and Table 7. MTF curves varied appreciably across scanners/acquisition protocols. Overall, GE-128, GE-64VCT and GE-16RT scanners were

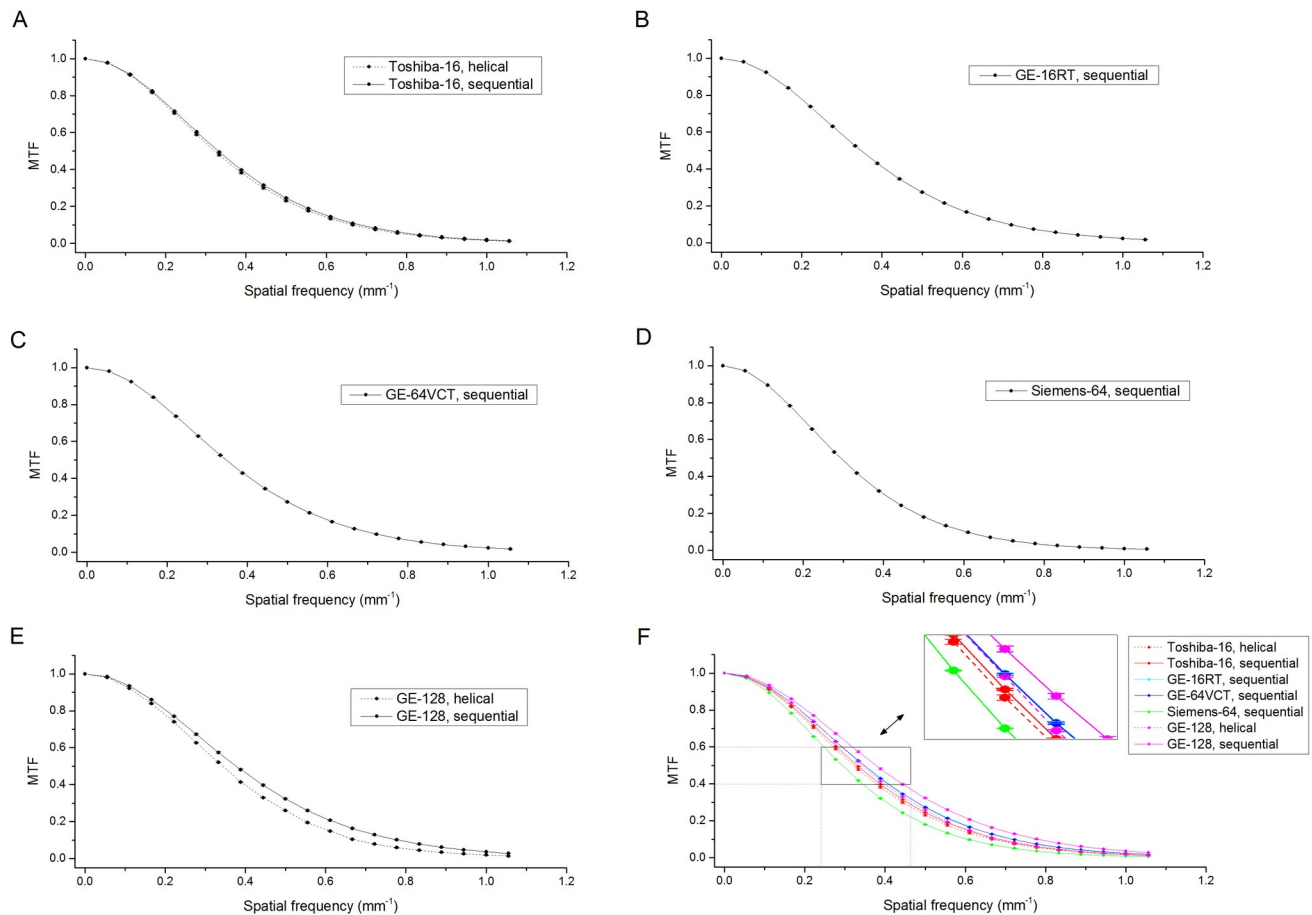


Fig 3. Modulation transfer function (MTF) curves of images acquired using different CT scanners/acquisitions protocols. Panels A, B, C, D and E show the MTF curves (mean ± standard deviation across five repeated measurements) for Toshiba-16, GE-16RT, GE-64VCT, Siemens-64 and GE-128 scanners, respectively. In order to better compare the different MTF curves, Panel F shows on the same graphic the MTF curves for all scanners/acquisition protocols, with a zoomed in version for the 40%-60% range of MTF.

<https://doi.org/10.1371/journal.pone.0245374.g003>

Table 7. Spatial frequencies (mean ± standard deviation across five repeated measurements) corresponding to 50% ($f_{50\%}$) and 10% ($f_{10\%}$) of the MTF curves, for each CT scanner/acquisition protocol.

Scanner ID	Scan mode	$f_{50\%}$ (mm ⁻¹)	$f_{10\%}$ (mm ⁻¹)
Toshiba-16	h	0.31 ± 0.01	0.66 ± 0.02
	s	0.31 ± 0.01	0.66 ± 0.02
GE-16RT	s	0.35 ± 0.01	0.65 ± 0.03
GE-64VCT	s	0.35 ± 0.01	0.65 ± 0.02
Siemens-64	s	0.28 ± 0.02	0.63 ± 0.03
GE-128	h	0.34 ± 0.01	0.67 ± 0.02
	s	0.38 ± 0.01	0.78 ± 0.02

h = helical, s = sequential.

<https://doi.org/10.1371/journal.pone.0245374.t007>

characterized by MTF curves with higher values with respect to the other scanners (Fig 3F). Specifically, GE-128 scanner with sequential acquisition protocol showed the best performance in terms of spatial resolution properties. The coefficient of variation of $f_{50\%}$ and $f_{10\%}$ across scanners/acquisition protocols was 10.1% and 7.4%, respectively.

A relevant difference in LCD performance of different scanners/acquisition protocols was found (Fig 4). For all object sizes, the Siemens-64 and GE-64VCT scanners showed lower contrast threshold values with respect to the other scanners. The contrast threshold for a typical object size of 3 mm ranged from 3.7 HU (Siemens-64 scanner) to 5.8 HU (Toshiba-16 scanner, sequential scan mode).

NUI results are reported in detail in Table 8. NUI values ranged from 4.1% (GE-128 scanner, sequential scan mode) to 8.3% (Toshiba-16 scanner, sequential scan mode) across different CT scanners/acquisition protocols.

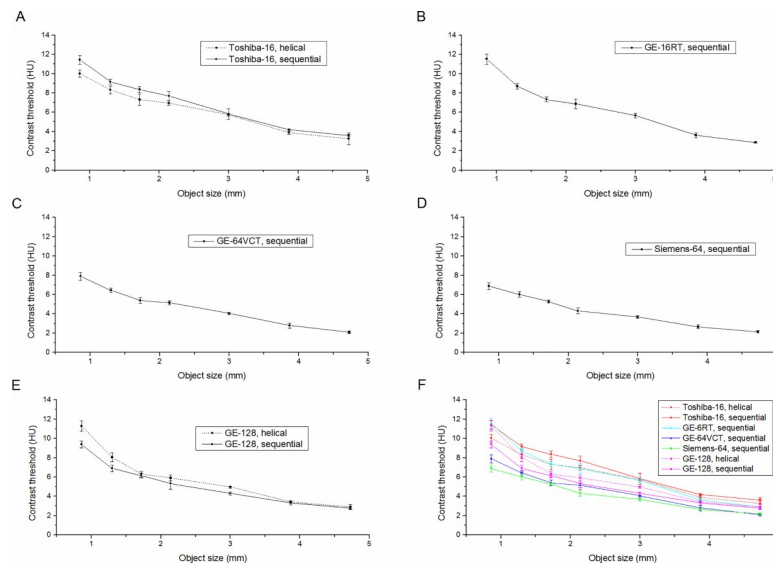


Fig 4. Low-contrast detectability (LCD) curves of images acquired using different CT scanners/acquisition protocols. Panels A, B, C, D and E show the LCD curves (mean ± standard deviation across five repeated measurements) for Toshiba-16, GE-16RT, GE-64VCT, Siemens-64 and GE-128 scanners, respectively. In order to better compare the different LCD curves, Panel F shows on the same graphic the LCD curves for all scanners/acquisition protocols.

<https://doi.org/10.1371/journal.pone.0245374.g004>

Table 8. NUI values (mean value \pm standard deviation across five repeated measurements) for each CT scanner/acquisition protocol.

Scanner ID	Scan mode	NUI (%)
Toshiba-16	h	7.6 \pm 0.2
	s	8.3 \pm 0.3
GE-16RT	s	7.5 \pm 0.3
GE-64VCT	s	8.0 \pm 0.2
Siemens-64	s	4.2 \pm 0.1
GE-128	h	4.2 \pm 0.2
	s	4.1 \pm 0.3

h = helical, s = sequential.

<https://doi.org/10.1371/journal.pone.0245374.t008>

4. Discussion

Nowadays, the technological advance in CT imaging has brought increasing number of clinical exams/applications, as well as increasing heterogeneity in characteristics/performance of CT scanners. Therefore, a number of CT scanners with different models or by different manufacturers are often installed in a hospital centre and used by various departments. Previous phantom studies, mainly focused on body applications, have shown that CT image quality can vary substantially across scanners [45–48], even when similar acquisition protocols are employed [49–52]. For instance, in a multicentre study, Racine et al [45] have compared the image quality of 68 scanners, in terms of only low contrast detectability, using local clinical acquisition protocols for abdominal CT examinations. They have found an important difference in image quality levels, associated with a variability in CTDI_{vol} values, which increased with growing phantom size. Kuo et al [47] have aimed at characterizing CT practices and performance of 16 CT scanners, in terms of noise and spatial resolution (i.e. MTF), in different centres for cystic fibrosis. A large variety in CT protocols, image quality and radiation dose among the centres was found. A task-based image quality assessment of 4 “older” (model released between 2003 and 2007) and 4 “newer” (model released between 2012 and 2014) CT scanners has been performed by another study [49], using similar acquisition protocols with fixed CTDI_{vol}. The authors have revealed an appreciable difference in high contrast spatial resolution and low contrast detectability across CT scanners. In the study by Zhang et al [50], both subjective and objective methods were used to evaluate the high contrast spatial resolution capabilities of three 64-slice CT scanners, using the same scanning parameters. The CT scanners exhibited different performances, which resulted more relevant for the subjective than the objective method for spatial resolution assessment. Solomon et al [52], using comparable acquisition protocols, have carried out a quantitative comparison of noise texture properties (i.e. NPS analysis) of two CT scanners, for a number of reconstruction filters. The peak frequency values ranged from 0.39 mm⁻¹ to 1.03 mm⁻¹ for one scanner and from 0.43 mm⁻¹ to 0.62 mm⁻¹ for the other.

To the best of our knowledge, this is the first phantom study which comprehensively assessed physical image quality of 5 different scanners (from various manufacturers) for head CT imaging at a single centre, considering the clinical acquisition protocols used by the staff of various Radiology/Neuroradiology departments of our hospital centre for routine examinations. Specifically, we performed an in-depth analysis of head CT image by using a number of quality indices such as noise level, NPS, CNR, MTF, LCD and NUI. Indeed, noise is one of the main factors affecting image quality, given that it can yield fluctuations in raw data and CT numbers. Noise level is usually estimated as the standard deviation of CT numbers within a

relatively small ROI. However, this approach does not consider any spatial relationship among fluctuations of CT numbers within the image. We have hence included, in our study, the analysis of NPS, which is mathematically defined as the Fourier transform of the autocorrelation function and provides information regarding the correlation of the fluctuations that occur at different positions on the image [38, 65, 67, 76, 78]. NPS is strictly related to the image appearance, i.e. image texture. Notably, different CT scanners/acquisition protocols can be characterized by different image textures, even at fixed noise level [66]. Moreover, noise can affect the detectability of an object, which depends on its contrast, as well as on its size. Therefore, for various contrast objects (teflon, delrin, LDPE, polystyrene, acrylic), we assessed CNR as the ratio between contrast (i.e. difference in CT numbers between the object and background) and noise [51, 67, 68, 79]. Furthermore, we included the LCD analysis, which allows to assess the limiting detectable contrast threshold for a given object size [71, 80–83]. In addition, the spatial resolution of CT scanner systems with varying spatial frequencies was evaluated by computing MTF, defined as the Fourier transform of the point spread function of the system, which represents the modulation/loss of contrast as a function of the spatial frequency due to the limited spatial resolution of the imaging system [61]. Therefore, MTF is a descriptive metric of the CT system performance in detecting objects with decreasing sizes (related to the inverse of spatial frequency of MTF). Moreover, in order to make our analysis more complete, we performed also the NUI analysis. NUI assesses the non-uniformity degree of CT numbers within the image, which can reflect the presence of potential artifacts (e.g. beam hardening).

In line with the findings of previous studies [45–52], we revealed appreciable differences in all CT image quality indices across scanners/acquisitions protocols. Noise level (Table 4), peak position of NPS curve (Table 5), $f_{50\%}$ (Table 7), $f_{10\%}$ (Table 7) and contrast threshold for a typical object size of 3 mm (Fig 4) differed across scanners/acquisition protocols up to 62.8%, 42.8%, 35.7%, 23.8% and 56.7%, respectively. Moreover, CNR values (Table 6) varied across CT scanners/acquisition protocols, with this effect resulting lower for the high contrast teflon insert as compared to the other contrast inserts. In particular, CNR values varied across CT scanners/acquisitions protocols up to 66.4%, 134.2%, 135.5%, 139.1% and 125.5% for teflon, delrin, LDPE, polystyrene and acrylic inserts, respectively. In addition, NUI values (Table 8) differed across scanners/acquisition protocols more than 100%.

While the head CT imaging acquisition protocols for the 5 scanners at our hospital centre were characterized by similar $CTDI_{vol}$ values (range: 54.7–57.5 mGy), there are some differences in various elements which include collimation (range: 8–20 mm), slice thickness (range: 2.5–6 mm) and reconstruction kernel (see Table 3). These differences can partly explain some results of noise, CNR and spatial resolution analyses [42, 52, 84, 85]. For instance, the relatively high slice thickness (6 mm) and soft reconstruction kernel (H31S) for acquisitions on the Siemens-64 scanner can contribute to the lower/higher noise/CNR values as well as to the lower spatial resolution properties with respect to the other scanners/acquisition protocols. Nonetheless, we cannot exclude a possible effect of scanner technology, as well as of some specific components of scanner hardware such as detectors and x-ray tube.

In the 5 CT scanners (from different manufacturers) enrolled in this study, given also the specific way of operating and needs of various Radiology/Neuroradiology departments of our hospital centre, different acquisition protocols for routine head CT examinations are employed, albeit they present similar $CTDI_{vol}$ values. We revealed a not negligible difference in CT image quality across scanners/acquisition protocols. As future research, our results can be useful to guide an optimization of head acquisition protocols for each CT scanner [42–44] or to possibly homogenize CT image quality across scanners. Nonetheless, given that a “best” or “worst” CT scanner/acquisition protocol for all image quality analyses was not found, the characterization that we performed can be potentially employed to allow a more appropriate

selection of a CT scanner/acquisition protocol for a specific clinical situation. In fact, different clinical applications may require specific image quality properties. For instance, higher performance of a CT scanner in terms of lower noise level are needed to optimize the detection of small haemorrhagic lesions. On the other hand, higher spatial resolution properties can improve metastatic brain lesions detection, while higher low contrast detectability properties are essential for a better interpretation of images acquired after ischemic stroke [86].

5. Conclusions

In this phantom study, a comprehensive assessment of image quality of 5 scanners (from various manufacturers and with different models) for head CT imaging, as clinically used at a single hospital centre, was performed. While similar clinical acquisition protocols in terms of dose value (i.e. $CTDI_{vol}$) were employed, the analysis of several quality indices (including noise level, NPS, CNR, MTF, LCD and NUI) has shown an appreciable and non-negligible variability in head CT imaging capabilities across different scanners/acquisition protocols. This highlights the importance of a physical characterization of each CT scanner/acquisition protocol, in order to optimize CT imaging procedures.

Author Contributions

Conceptualization: Patrizio Barca, Marco Giannelli.

Data curation: Patrizio Barca.

Formal analysis: Patrizio Barca, Daniela Marfisi.

Investigation: Patrizio Barca, Fabio Paolicchi.

Methodology: Patrizio Barca, Marco Giannelli.

Resources: Davide Caramella.

Software: Patrizio Barca, Daniela Marfisi.

Supervision: Marco Giannelli.

Validation: Patrizio Barca, Fabio Paolicchi, Giacomo Aringhieri, Federica Palmas, Daniela Marfisi, Maria Evelina Fantacci, Davide Caramella, Marco Giannelli.

Visualization: Patrizio Barca, Fabio Paolicchi, Giacomo Aringhieri, Federica Palmas, Daniela Marfisi, Maria Evelina Fantacci, Davide Caramella, Marco Giannelli.

Writing – original draft: Patrizio Barca, Marco Giannelli.

Writing – review & editing: Patrizio Barca, Davide Caramella, Marco Giannelli.

References

1. Seeram E. Computed tomography: physical principles, clinical applications, and quality control. Fourth edition. St. Louis, Missouri: Elsevier; 2016.
2. Kalender W. Computed tomography: fundamentals, system technology, image quality, applications. Weinheim: Wiley-VCH; 2011.
3. Liguori C, Frauenfelder G, Massaroni C, Saccomandi P, Giurazza F, Pitocco F, et al. Emerging clinical applications of computed tomography. *Med Devices (Auckl)*. 2015; 8: 265–278. <https://doi.org/10.2147/MDER.S70630> PMID: 26089707
4. European Commission, Directorate-General for Energy. Medical radiation exposure of the European population. Luxembourg: Publications Office; 2015.

5. National Council on Radiation Protection and Measurements. Ionizing radiation exposure of the population of the United States: recommendations of the National Council on Radiation Protection and Measurements. NCRP Report N° 160; 2009.
6. Brenner DJ, Hall EJ. Computed tomography—An increasing source of radiation exposure. *N Engl J Med*. 2007; 357: 2277–2284. <https://doi.org/10.1056/NEJMra072149> PMID: 18046031
7. Trattner S, Pearson GDN, Chin C, Cody DD, Gupta R, Hess CP, et al. Standardization and optimization of CT protocols to achieve low dose. *J Am Coll Radiol*. 2014; 11: 271–278. <https://doi.org/10.1016/j.jacr.2013.10.016> PMID: 24589403
8. Kofler JM, Cody DD, Morin RL. CT protocol review and optimization. *J Am Coll Radiol*. 2014; 11: 267–270. <https://doi.org/10.1016/j.jacr.2013.10.013> PMID: 24589402
9. Zhang Y, Smitherman C, Samei E. Size-specific optimization of CT protocols based on minimum detectability. *Med Phys*. 2017; 44: 1301–1311. <https://doi.org/10.1002/mp.12125> PMID: 28122119
10. Kalender WA, Buchenau S, Deak P, Kellermeier M, Langner O, van Straten M, et al. Technical approaches to the optimisation of CT. *Phys Med*. 2008; 24: 71–79. <https://doi.org/10.1016/j.ejmp.2008.01.012> PMID: 18331808
11. Ohno Y, Koyama H, Seki S, Kishida Y, Yoshikawa T. Radiation dose reduction techniques for chest CT: Principles and clinical results. *Eur Radiol*. 2019; 111: 93–103. <https://doi.org/10.1016/j.ejrad.2018.12.017> PMID: 30691672
12. Higaki T, Nakamura Y, Fukumoto W, Honda Y, Tatsugami F, Awai K. Clinical application of radiation dose reduction at abdominal CT. *Eur J Radiol*. 2019; 111: 68–75. <https://doi.org/10.1016/j.ejrad.2018.12.018> PMID: 30691668
13. Nagayama Y, Oda S, Nakaura T, Tsuji A, Urata J, Furusawa M, et al. Radiation dose reduction at pediatric CT: Use of low tube voltage and iterative reconstruction. *Radiographics*. 2018; 38: 1421–1440. <https://doi.org/10.1148/rg.2018180041> PMID: 30207943
14. Zinsser D, Marcus R, Othman A, Bamberg F, Nikolaou K, Flohr T, et al. Dose reduction and dose management in computed tomography—state of the art. *Rofo*. 2018; 190: 531–541. <https://doi.org/10.1055/s-0044-101261> PMID: 29534253
15. Hedgire S, Ghoshhajra B, Kalra M. Dose optimization in cardiac CT. *Phys Med*. 2017; 41: 97–103. <https://doi.org/10.1016/j.ejmp.2017.04.021> PMID: 28506649
16. Santos J, Batista M do C, Foley S, Paulo G, McEntee MF, Rainford L. Paediatric CT optimisation utilising Catphan® 600 and age-specific anthropomorphic phantoms. *Radiat Prot Dosimetry*. 2014; 162: 586–596. <https://doi.org/10.1093/rpd/ncu018> PMID: 24567497
17. Yu L, Primak AN, Liu X, McCollough CH. Image quality optimization and evaluation of linearly mixed images in dual-source, dual-energy CT. *Med Phys*. 2009; 36: 1019–1024. <https://doi.org/10.1118/1.3077921> PMID: 19378762
18. Niiniviita H, Salminen P, Grönroos JM, Rinta-Kiikka I, Hurme S, Kiljunen T, et al. Low-dose ct protocol optimization for the assessment of acute appendicitis: The OPTICAP phantom study. *Radiat Prot Dosimetry*. 2018; 178: 20–28. <https://doi.org/10.1093/rpd/ncx070> PMID: 28591824
19. Berta L, Mascaro L, Feroldi P, Maroldi R. Optimisation of an MDCT abdominal protocol: Image quality assessment of standard vs. iterative reconstructions. *Phys Med*. 2014; 30: 271–279. <https://doi.org/10.1016/j.ejmp.2013.07.126> PMID: 23948366
20. Greffier J, Macri F, Larbi A, Fernandez A, Khasanova E, Pereira F, et al. Dose reduction with iterative reconstruction: Optimization of CT protocols in clinical practice. *Diagn Interv Imaging*. 2015; 96: 477–486. <https://doi.org/10.1016/j.diii.2015.02.007> PMID: 25797211
21. Noferini L, Taddeucci A, Bartolini M, Bruschi A, Menchi I. CT image quality assessment by a Channelized Hotelling Observer (CHO): Application to protocol optimization. *Phys Med*. 2016; 32: 1717–1723. <https://doi.org/10.1016/j.ejmp.2016.11.002> PMID: 27964873
22. Nute JL, Jacobsen MC, Stefan W, Wei W, Cody DD. Development of a dual-energy computed tomography quality control program: Characterization of scanner response and definition of relevant parameters for a fast-kVp switching dual-energy computed tomography system. *Med Phys*. 2018; 45: 1444–1458. <https://doi.org/10.1002/mp.12812> PMID: 29446082
23. Hassan AI, Skalej M, Schlattl H, Hoeschen C. Determination and verification of the x-ray spectrum of a CT scanner. *J Med Imag*. 2018; 5: 1. <https://doi.org/10.1117/1.JMI.5.1.013506> PMID: 29430476
24. Ozguner O, Dhanantwari A, Halliburton S, Wen G, Utrup S, Jordan D. Objective image characterization of a spectral CT scanner with dual-layer detector. *Phys Med Biol*. 2018; 63: 025027. <https://doi.org/10.1088/1361-6560/aa9e1b> PMID: 29185436
25. Weir VJ, Zhang J, Bruner AP. Dosimetric characterization and image quality evaluation of the AIRO mobile CT scanner. *J Xray Sci Technol*. 2015; 23: 373–381. <https://doi.org/10.3233/XST-150496> PMID: 26410470

26. Cropp RJ, Seslija P, Tso D, Thakur Y. Scanner and kVp dependence of measured CT numbers in the ACR CT phantom. *J Appl Clin Med Phys*. 2013; 14: 338–349. <https://doi.org/10.1120/jacmp.v14i6.4417> PMID: 24257284
27. Garcia-Ramirez JL, Mucic S, Dempsey JF, Low DA, Purdy JA. Performance evaluation of an 85-cm-bore X-ray computed tomography scanner designed for radiation oncology and comparison with current diagnostic CT scanners. *Int J Radiat Oncol Biol Phys*. 2002; 52: 1123–1131. [https://doi.org/10.1016/s0360-3016\(01\)02779-1](https://doi.org/10.1016/s0360-3016(01)02779-1) PMID: 11958910
28. Husby E, Svendsen ED, Andersen HK, Martinsen ACT. 100 days with scans of the same Catphan phantom on the same CT scanner. *J Appl Clin Med Phys*. 2017; 18: 224–231. <https://doi.org/10.1002/acm2.12186> PMID: 28921910
29. Chen-Mayer HH, Fuld MK, Hoppel B, Judy PF, Sieren JP, Guo J, et al. Standardizing CT lung density measure across scanner manufacturers. *Med Phys*. 2017; 44: 974–985. <https://doi.org/10.1002/mp.12087> PMID: 28060414
30. Zambelli J, Bevins N, Qi Z, Chen G-H. Radiation dose efficiency comparison between differential phase contrast CT and conventional absorption CT. *Med Phys*. 2010; 37: 2473–2479. <https://doi.org/10.1118/1.3425785> PMID: 20632558
31. Christner JA, Stierstorfer K, Primak AN, Eusemann CD, Flohr TG, McCollough CH. Evaluation of z-axis resolution and image noise for nonconstant velocity spiral CT data reconstructed using a weighted 3D filtered backprojection (WFBP) reconstruction algorithm. *Med Phys*. 2010; 37: 897–906. <https://doi.org/10.1118/1.3271110> PMID: 20229899
32. Flohr TG, Stierstorfer K, Ulzheimer S, Bruder H, Primak AN, McCollough CH. Image reconstruction and image quality evaluation for a 64-slice CT scanner with z-flying focal spot. *Med Phys*. 2005; 32: 2536–2547. <https://doi.org/10.1118/1.1949787> PMID: 16193784
33. Papadakis AE, Damilakis J. Automatic Tube Current Modulation and Tube Voltage Selection in Pediatric Computed Tomography: A Phantom Study on Radiation Dose and Image Quality. *Invest Radiol*. 2019; 54: 265–272. <https://doi.org/10.1097/RLI.0000000000000537> PMID: 30562273
34. Greffier J, Pereira F, Macri F, Beregi J-P, Larbi A. CT dose reduction using Automatic Exposure Control and iterative reconstruction: A chest paediatric phantoms study. *Phys Med*. 2016; 32: 582–589. <https://doi.org/10.1016/j.ejmp.2016.03.007> PMID: 27056436
35. Papadakis AE, Perisinakis K, Raissaki M, Damilakis J. Effect of X-ray Tube parameters and iodine concentration on image quality and radiation dose in cerebral pediatric and adult CT angiography: A phantom study. *Invest Radiol*. 2013; 48: 192–199. <https://doi.org/10.1097/RLI.0b013e31827efc17> PMID: 23344518
36. Barca P, Giannelli M, Fantacci ME, Caramella D. Computed tomography imaging with the Adaptive Statistical Iterative Reconstruction (ASiR) algorithm: dependence of image quality on the blending level of reconstruction. *Australas Phys Eng Sci Med*. 2018; 41: 463–473. <https://doi.org/10.1007/s13246-018-0645-8> PMID: 29737491
37. De Marco P, Origgi D. New adaptive statistical iterative reconstruction ASiR-V: Assessment of noise performance in comparison to ASiR. *J Appl Clin Med Phys*. 2018; 19: 275–286. <https://doi.org/10.1002/acm2.12253> PMID: 29363260
38. Li K, Tang J, Chen G-H. Statistical model based iterative reconstruction (MBiR) in clinical CT systems: Experimental assessment of noise performance. *Med Phys*. 2014; 41: 041906. <https://doi.org/10.1118/1.4867863> PMID: 24694137
39. Li K, Garrett J, Ge Y, Chen G-H. Statistical model based iterative reconstruction (MBiR) in clinical CT systems. Part II. Experimental assessment of spatial resolution performance. *Med Phys*. 2014; 41: 071911. <https://doi.org/10.1118/1.4884038> PMID: 24989389
40. Viry A, Aberle C, Racine D, Knebel J-F, Schindera ST, Schmidt S, et al. Effects of various generations of iterative CT reconstruction algorithms on low-contrast detectability as a function of the effective abdominal diameter: A quantitative task-based phantom study. *Phys Med*. 2018; 48: 111–118. <https://doi.org/10.1016/j.ejmp.2018.04.006> PMID: 29728223
41. Li H, Dolly S, Chen H-C, Anastasio MA, Low DA, Li HH, et al. A comparative study based on image quality and clinical task performance for CT reconstruction algorithms in radiotherapy. *J Appl Clin Med Phys*. 2016; 17: 377–390. <https://doi.org/10.1120/jacmp.v17i4.5763> PMID: 27455472
42. Winslow J, Zhang Y, Samei E. A method for characterizing and matching CT image quality across CT scanners from different manufacturers. *Med Phys*. 2017; 44: 5705–5717. <https://doi.org/10.1002/mp.12554> PMID: 28865170
43. Chen B, Ramirez Giraldo JC, Solomon J, Samei E. Evaluating iterative reconstruction performance in computed tomography. *Med Phys*. 2014; 41: 121913. <https://doi.org/10.1118/1.4901670> PMID: 25471973

44. Christianson O, Chen JJS, Yang Z, Saiprasad G, Dima A, Filliben JJ, et al. An improved index of image quality for task-based performance of CT iterative reconstruction across three commercial implementations. *Radiology*. 2015; 275: 725–734. <https://doi.org/10.1148/radiol.15132091> PMID: 25686365
45. Racine D, Ryckx N, Ba A, Becce F, Viry A, Verdun FR, et al. Task-based quantification of image quality using a model observer in abdominal CT: a multicentre study. *Eur Radiol*. 2018; 28: 5203–5210. <https://doi.org/10.1007/s00330-018-5518-8> PMID: 29858638
46. Niiniviita H, Kiljunen T, Kulmala J. Comparison of effective dose and image quality for newborn imaging on seven commonly used CT scanners. *Radiat Prot Dosimetry*. 2016; rpd;ncw229v1. <https://doi.org/10.1093/rpd/ncw229> PMID: 27522051
47. Kuo W, Kemner-van de Corput MPC, Perez-Rovira A, de Bruijne M, Fajac I, Tiddens HAWM, et al. Multicentre chest computed tomography standardisation in children and adolescents with cystic fibrosis: the way forward. *Eur Respir J*. 2016; 47: 1706–1717. <https://doi.org/10.1183/13993003.01601-2015> PMID: 27076593
48. Scheck RJ, Coppenrath EM, Kellner MW, Lehmann KJ, Rock C, Rieger J, et al. Radiation dose and image quality in spiral computed tomography: multicentre evaluation at six institutions. *Br J Radiol*. 1998; 71: 734–744. <https://doi.org/10.1259/bjr.71.847.9771384> PMID: 9771384
49. Racine D, Viry A, Becce F, Schmidt S, Ba A, Bochud FO, et al. Objective comparison of high-contrast spatial resolution and low-contrast detectability for various clinical protocols on multiple CT scanners. *Med Phys*. 2017; 44: e153–e163. <https://doi.org/10.1002/mp.12224> PMID: 28901621
50. Zhang P, Wan G, Li F, Li X, Liu W, Wang G. A novel objective method for assessing high-contrast spatial resolution in CT based on the Rayleigh criterion. *Med Phys*. 2017; 44: 460–469. <https://doi.org/10.1002/mp.12070> PMID: 28019671
51. Roa AMA, Andersen HK, Martinsen ACT. CT image quality over time: comparison of image quality for six different CT scanners over a six-year period. *J Appl Clin Med Phys*. 2015; 16: 350–365. <https://doi.org/10.1120/jacmp.v16i2.4972> PMID: 26103172
52. Solomon JB, Christianson O, Samei E. Quantitative comparison of noise texture across CT scanners from different manufacturers. *Med Phys*. 2012; 39: 6048–6055. <https://doi.org/10.1118/1.4752209> PMID: 23039643
53. Wang X, You JJ. Head CT for nontrauma patients in the emergency department: clinical predictors of abnormal findings. *Radiology*. 2013; 266: 783–790. <https://doi.org/10.1148/radiol.12120732> PMID: 23204540
54. Haydel MJ, Preston CA, Mills TJ, Luber S, Blaudeau E, DeBlieux PMC. Indications for computed tomography in patients with minor head injury. *N Engl J Med*. 2000; 343: 100–105. <https://doi.org/10.1056/NEJM200007133430204> PMID: 10891517
55. Hosten N, Liebig T. *CT of the head and spine*. Stuttgart: Thieme; 2011.
56. Kloska SP, Nabavi DG, Gaus C, Nam E-M, Klotz E, Ringelstein EB, et al. Acute stroke assessment with CT: Do we need multimodal evaluation? *Radiology*. 2004; 233: 79–86. <https://doi.org/10.1148/radiol.2331030028> PMID: 15340177
57. Lell MM, Anders K, Uder M, Klotz E, Ditt H, Vega-Higuera F, et al. New techniques in CT angiography. *Radiographics*. 2006; 26: S45–S62. <https://doi.org/10.1148/rg.26si065508> PMID: 17050518
58. The Phantom Laboratory. *Catphan® 504 Manual*. 2013.
59. Buzug TM. *Computed tomography: from photon statistics to modern cone-beam CT*. Berlin: Springer; 2010.
60. Dance DR. *Diagnostic radiology physics: a handbook for teachers and students*. Vienna: International Atomic Energy Agency; 2014.
61. Bushberg JT. *The essential physics of medical imaging*. 3rd ed. Philadelphia: Wolters Kluwer Health/Lippincott Williams & Wilkins; 2012. <https://doi.org/10.1109/TMI.2012.2216890> PMID: 22961298
62. Brahme A. *Comprehensive biomedical physics*. Amsterdam: Elsevier; 2014.
63. Samei E, Pelc NJ. *Computed tomography: approaches, applications, and operations*. Springer International Publishing; 2020.
64. Hsieh J. *Computed tomography: Principles, design, artifacts and recent advances*. SPIE PRESS; 2015. <https://doi.org/10.1117/3.2197756>
65. Friedman SN, Fung GSK, Siewerdsen JH, Tsui BMW. A simple approach to measure computed tomography (CT) modulation transfer function (MTF) and noise-power spectrum (NPS) using the American College of Radiology (ACR) accreditation phantom. *Med Phys*. 2013; 40: 051907. <https://doi.org/10.1118/1.4800795> PMID: 23635277

66. Siewerdsen JH, Cunningham IA, Jaffray DA. A framework for noise-power spectrum analysis of multidimensional images. *Med Phys*. 2002; 29: 2655–2671. <https://doi.org/10.1118/1.1513158> PMID: [12462733](https://pubmed.ncbi.nlm.nih.gov/12462733/)
67. Kawashima H, Ichikawa K, Hanaoka S, Matsubara K, Takata T. Relationship between size-specific dose estimates and image quality in computed tomography depending on patient size. *J Appl Clin Med Phys*. 2018; 19: 246–251. <https://doi.org/10.1002/acm2.12340> PMID: [29729075](https://pubmed.ncbi.nlm.nih.gov/29729075/)
68. Pontana F, Duhamel A, Pagniez J, Flohr T, Faivre J-B, Hachulla A-L, et al. Chest computed tomography using iterative reconstruction vs filtered back projection (Part 2): image quality of low-dose CT examinations in 80 patients. *Eur Radiol*. 2011; 21: 636–643. <https://doi.org/10.1007/s00330-010-1991-4> PMID: [21080171](https://pubmed.ncbi.nlm.nih.gov/21080171/)
69. Takenaga T, Katsuragawa S, Goto M, Hatemura M, Uchiyama Y, Shiraishi J. Modulation transfer function measurement of CT images by use of a circular edge method with a logistic curve-fitting technique. *Radiol Phys Technol*. 2015; 8: 53–59. <https://doi.org/10.1007/s12194-014-0286-x> PMID: [25142743](https://pubmed.ncbi.nlm.nih.gov/25142743/)
70. Spadavecchia C, Villa R, Pasquali C, Paruccini N, Oberhofer N, Crespi A. A statistical method for low contrast detectability assessment in digital mammography. In: Tingberg A, Lång K, Timberg P. *Breast Imaging*. Springer International Publishing; 2016. pp. 532–539. https://doi.org/10.1007/978-3-319-41546-8_67
71. Torgersen GR, Hol C, Møystad A, Hellén-Halme K, Nilsson M. A phantom for simplified image quality control of dental cone beam computed tomography units. *Oral Surg Oral Med Oral Pathol Oral Radiol*. 2014; 118: 603–611. <https://doi.org/10.1016/j.oooo.2014.08.003> PMID: [25442498](https://pubmed.ncbi.nlm.nih.gov/25442498/)
72. Rose A. Television pickup tubes and the problem of vision. *Advances in electronics and electron physics*. Elsevier; 1948. pp. 131–166. [https://doi.org/10.1016/S0065-2539\(08\)61102-6](https://doi.org/10.1016/S0065-2539(08)61102-6)
73. Rose A. Quantum effects in human vision. *Adv Biol Med Phys*. 1957; 5: 211–242. <https://doi.org/10.1016/b978-1-4832-3111-2.50009-2> PMID: [13520432](https://pubmed.ncbi.nlm.nih.gov/13520432/)
74. Rose A. *Vision: human and electronic*. New York: Plenum Press; 1973.
75. Burgess AE. The Rose model, revisited. *J Opt Soc Am A*. 1999; 16: 633. <https://doi.org/10.1364/josaa.16.000633> PMID: [10069050](https://pubmed.ncbi.nlm.nih.gov/10069050/)
76. Verdun FR, Racine D, Ott JG, Tapiovaara MJ, Toroi P, Bochud FO, et al. Image quality in CT: From physical measurements to model observers. *Phys Med*. 2015; 31: 823–843. <https://doi.org/10.1016/j.ejmp.2015.08.007> PMID: [26459319](https://pubmed.ncbi.nlm.nih.gov/26459319/)
77. Samei E, Bakalyar D, Boedeker K, Brady S, Fan J, Leng S, et al. Performance evaluation of computed tomography systems—The report of AAPM task group 233. *AAPM*; 2019 Nov. <https://doi.org/10.37206/186>
78. Samei E, Richard S. Assessment of the dose reduction potential of a model-based iterative reconstruction algorithm using a task-based performance metrology. *Med Phys*. 2014; 42: 314–323. <https://doi.org/10.1118/1.4903899> PMID: [25563271](https://pubmed.ncbi.nlm.nih.gov/25563271/)
79. Rotzinger DC, Racine D, Beigelman-Aubry C, Alfudhili KM, Keller N, Monnin P, et al. Task-Based model observer assessment of a partial model-based iterative reconstruction algorithm in thoracic oncologic multidetector CT. *Sci Rep*. 2018; 8: 17734. <https://doi.org/10.1038/s41598-018-36045-4> PMID: [30531988](https://pubmed.ncbi.nlm.nih.gov/30531988/)
80. Hernandez-Giron I, Geleijns J, Calzado A, Veldkamp WJH. Automated assessment of low contrast sensitivity for CT systems using a model observer. *Med Phys*. 2011; 38: S25–S35. <https://doi.org/10.1118/1.3577757> PMID: [21978115](https://pubmed.ncbi.nlm.nih.gov/21978115/)
81. Kofler JM, Yu L, Leng S, Zhang Y, Li Z, Carter RE, et al. Assessment of low-contrast resolution for the American College of Radiology computed tomographic accreditation program: What is the impact of iterative reconstruction? *J Comput Assist Tomogr*. 2015; 39: 619–623. <https://doi.org/10.1097/RCT.000000000000245> PMID: [25853774](https://pubmed.ncbi.nlm.nih.gov/25853774/)
82. Bellesi L, Wyttenbach R, Gaudino D, Colleoni P, Pupillo F, Carrara M, et al. A simple method for low-contrast detectability, image quality and dose optimisation with CT iterative reconstruction algorithms and model observers. *Eur Radiol Exp*. 2017; 1: 18. <https://doi.org/10.1186/s41747-017-0023-4> PMID: [29708194](https://pubmed.ncbi.nlm.nih.gov/29708194/)
83. Brisse HJ, Brenot J, Pierrat N, Gaboriaud G, Savignoni A, De Rycke Y, et al. The relevance of image quality indices for dose optimization in abdominal multi-detector row CT in children: experimental assessment with pediatric phantoms. *Phys Med Biol*. 2009; 54: 1871–1892. <https://doi.org/10.1088/0031-9155/54/7/002> PMID: [19265204](https://pubmed.ncbi.nlm.nih.gov/19265204/)
84. Eldevik K, Nordhoy W, Skretting A. Relationship between sharpness and noise in CT images reconstructed with different kernels. *Radiat Prot Dosimetry*. 2010; 139: 430–433. <https://doi.org/10.1093/rpd/ncq063> PMID: [20181647](https://pubmed.ncbi.nlm.nih.gov/20181647/)

85. Sookpeng S, Martin CJ, Gentle DJ. Investigation of the influence of image reconstruction filter and scan parameters on operation of automatic tube current modulation systems for different CT scanners. *Radiat Prot Dosimetry*. 2015; 163: 521–530. <https://doi.org/10.1093/rpd/ncu236> PMID: 25107439
86. von Kummer R, Bourquain H, Bastianello S, Bozzao L, Manelfe C, Meier D, et al. Early prediction of irreversible brain damage after ischemic stroke at CT. *Radiology*. 2001; 219: 95–100. <https://doi.org/10.1148/radiology.219.1.r01ap0695> PMID: 11274542